AGU PUBLICATIONS

Journal of Advances in Modeling Earth Systems

RESEARCH ARTICLE
10.1002/2017MS001113

Can We Use Single-Column Models for Understanding the Boundary Layer Cloud-Climate Feedback?

S. Dal Gesso[1] and R. A. J. Neggers[1]

[1]Institute of Geophysics and Meteorology, University of Cologne, Cologne, Germany

Key Points:
- High-frequency output of GCMs is used as prescribed large-scale forcings in long-term SCM simulations of the Caribbean dry season
- The free troposphere is kept in approximate radiative-advective equilibrium, while the fast boundary layer physics are free to act
- The low-level clouds of the GCM in current climate and their response to a climate perturbation are both reproduced with this method

Correspondence to:
S. Dal Gesso,
dalgesso@meteo.uni-koeln.de

Citation:
Dal Gesso, S., & Neggers, R. A. J. (2018). Can we use single-column models for understanding the boundary layer cloud-climate feedback? *Journal of Advances in Modeling Earth Systems*, *10*, 245–261. https://doi.org/10.1002/2017MS001113

Received 3 JUL 2017
Accepted 5 DEC 2017
Accepted article online 14 DEC 2017
Published online 1 FEB 2018

Abstract This study explores how to drive Single-Column Models (SCMs) with existing data sets of General Circulation Model (GCM) outputs, with the aim of studying the boundary layer cloud response to climate change in the marine subtropical trade wind regime. The EC-EARTH SCM is driven with the large-scale tendencies and boundary conditions as derived from two different data sets, consisting of high-frequency outputs of GCM simulations. SCM simulations are performed near Barbados Cloud Observatory in the dry season (January–April), when fair-weather cumulus is the dominant low-cloud regime. This climate regime is characterized by a near equilibrium in the free troposphere between the long-wave radiative cooling and the large-scale advection of warm air. In the SCM, this equilibrium is ensured by scaling the monthly mean dynamical tendency of temperature and humidity such that it balances that of the model physics in the free troposphere. In this setup, the high-frequency variability in the forcing is maintained, and the boundary layer physics acts freely. This technique yields representative cloud amount and structure in the SCM for the current climate. Furthermore, the cloud response to a sea surface warming of 4 K as produced by the SCM is consistent with that of the forcing GCM.

Plain Language Summary The cloud response to climate change remains one of the main uncertainties in the predictions of climate models. Shallow-cumulus clouds have been identified as the cloud regime that contributes the most to the inter-model spread. This is due to both their key importance in the climate system and to their persistent occurrence all over the globe. To move forward, it is indeed necessary to gain insight into the reasons of the inter-model differences. This article presents a new method aimed to tackle this problem. The analysis explores the advantages and the applicability of this novel technique. The results prove that such a method is an effective way to exploit existing data sets for testing climate models and for increasing our understanding in the shallow-cumulus clouds response.

1. Introduction

Shallow-cumulus clouds are a fundamental component of the climate system. Widely present all over the globe, they prevail in the Trades over the Tropical oceans. Their effect on climate is twofold: on the one hand, they have a key role in the moisture transport toward the equator, contributing to the formation of deep convective clouds; on the other, they are crucial contributors in the energy budget of the planet (Stephens et al., 2012). They are characterized by a relatively high reflectivity to incoming solar radiation, as compared to the underlying earth surface. At the same time, their limited interaction with the terrestrial radiation entails a cooling effect (Hartmann et al., 1992). Because of their persistent presence throughout the tropics, their overall contribution to the global albedo is significant.

The representation of shallow-cumulus clouds in General Circulation Models (GCMs) is a long-standing challenge (e.g., Nam et al., 2012). With their horizontal extent smaller than the resolution of GCMs, they are not directly resolved, but result from a suite of parameterizations. Such parameterizations interact with the resolved large-scale (LS) dynamics in complex ways. A complicating factor is the broad range of time scales that is involved, ranging from subdiurnal feedbacks to climate time scales. As a result, this cloud regime is the major contributor to the inter-model spread in the climate sensitivity predictions (e.g., Bony & Dufresne, 2005; Vial et al., 2013).

Several recent studies investigate the physical mechanisms underlying the boundary layer (BL) cloud response to climate change in GCMs. Based on Zhang and Bretherton (2008), the Cloud Feedback Model Intercomparison Project - Global System Atmospheric Studies (CFMIP-GASS) Intercomparison of Large Eddy Models (LESs) and Single-Column Models (SCMs), CGILS, has been set up (Blossey et al., 2013; Zhang et al., 2013). This intercomparison project entails three cloud regimes: well-mixed stratocumulus, decoupled stratocumulus, and shallow cumulus. For each regime, it includes the steady state LS forcing conditions of a control experiment and an idealized climate perturbation. One of the key conclusions of this study is that the cloud response simulated by the SCMs is not necessarily representative of the parent GCM. This implies that using SCMs in this setup to gain insight into the inter-model spread in the GCM predictions is not straightforward.

Further attempts have been made to improve the CGILS method of using SCMs by extending it in two ways. Brient and Bony (2012) include a stochastic component into the LS subsidence to mimic the climate variability. In this way, the SCM results are representative of the parent GCM. However, this method has been tested with one model and on one case, and, until now, it is not yet clear whether it is more widely applicable. More specifically, a *general* method for defining an artificial noise which mimics the climate variability and ensures that the SCM is representative of the parent GCM has not been identified yet.

Dal Gesso et al. (2014, 2015a) generalize the CGILS experiment by considering a range of free-tropospheric thermodynamic conditions. Each of the considered conditions corresponds to a steady state, and through the analysis of all the solutions, a whole phase space is explored. On the basis of this framework, a model intercomparison study has been set up (Dal Gesso et al., 2015b). Although this method reduces the spread among SCM results with respect to CGILS, the estimated cloud feedback is still not representative of the parent GCM. These results suggest that the setups considered until now might be too idealized to represent the whole complexity of the climate system.

Another possible approach is to drive the SCM directly with high-temporal resolution outputs of a GCM. In this way, realistic estimates of the natural high-frequency variability are automatically included, not just for one forcing variable but for many variables at the same time. However, existing data sets might not include all the outputs necessary or might not be suitable for driving a specific SCM. It is therefore important to develop a framework for studying the cloud-climate feedback that exploits existing data sets. This is the main goal of this article, which describes a novel technique to force a SCM to obtain a cloud response, which is representative of that of the parent GCM.

The physical basis of the method presented in this article is described in section 2. A brief overview of the SCM and of the forcing data sets is given in section 3, followed by the description of the experimental setup. The SCM results are reported in section 5. Finally, conclusions and outlook are summarized in section 6.

2. Radiative-Advective Equilibrium in the Trades

2.1. The Barbados Cloud Observatory

This study focuses on the Caribbean Trades because of the persistent occurrence of shallow cumulus throughout the year. More precisely, the analysis is conducted near Barbados Cloud Observatory (BCO, 13.15°N, 59.4°W), which is a permanent meteorological site with a continuous record of cloud observations since 2010 (Nuijens et al., 2014). This site has been selected for several reasons. First, Medeiros and Nuijens (2016) show that the climatological conditions and the cloud properties measured at BCO are representative of the Trades. Second, the cloud fields of this region have been widely investigated in field campaigns (e.g., Nitta & Esbensen, 1974; Rauber et al., 2007) and in model studies (e.g., Nuijens et al., 2015; Siebesma & Cuijpers, 1995; Vanzanten et al., 2011). Last, the extensive BCO observations provide opportunities for future model evaluation efforts.

BCO presents a very distinct seasonality. The boreal winter exhibits LS conditions that prevent the formation of deep convection, such as a LS subsidence, a strong capping inversion at the BL top, and a relatively cold sea surface temperature (SST). By contrast, the boreal summer is affected by the northward shift of the Inter-Tropical Convergence Zone, which results in LS ascent and a weakening of the temperature gradient at the BL top. These conditions facilitate the formation of deep and precipitative convective clouds. For

distinguishing between these regimes, the seasonality is divided into the dry and wet season (Stevens et al., 2016).

We restrict our analysis to the *dry season*, defined as the period between January and April, following Brueck et al. (2015). The reason for this choice is twofold: on the one hand, the focus of this study is on BL clouds, which are dominant in the dry season (Medeiros & Nuijens, 2016); on the other, the SCM is not ideally suited for simulating deep convection because, in its standard setup, it does not include the direct feedback of the deep convection on the dynamics. More complex setups allowing for the deep cumulus regime, such as the application of the weak temperature gradient method (e.g., Ruppert, 2016; Sobel et al., 2007), will be considered in future work.

2.2. Definition of Radiative-Advective Equilibrium

During the dry season at BCO, the free troposphere is in a near equilibrium between the net long-wave radiative cooling and the warming due to advective transport. We refer to this balance as the *Radiative-Advective Equilibrium* (RAE; Cronin & Jansen, 2016). RAE is similar to the concept of Radiative-Convective Equilibrium (RCE), in the sense that an approximate balance exists in the free troposphere between two dominating processes. However, one essential difference exists. On the one hand, RCE involves a *negative* feedback that ensures equilibration. When a continuous cooling enhances instability, convection intensifies to quickly overturn and reduce it, by which it quickly reduces its own intensity again. By contrast, with RAE this is not the case, because a perturbation in the LS advective transport does not automatically trigger an immediate and quick response in the radiative tendency.

In a SCM, structural imbalances between these two dominant but independent processes may lead to a significant drift in the thermodynamic state in the free troposphere. It is hence important to ensure RAE, without overly constraining the other physical processes that control the evolution of shallow-cumulus clouds. How to achieve this fine balance is explored in this study.

2.3. Ensuring RAE in a SCM

In this section, we introduce a method for imposing RAE. As a first step, we discuss in detail the temperature budget once RAE is achieved, which is schematically depicted in Figure 1. The left-hand side plot illustrates the temperature (T) structure and all the active process at different heights. The right-hand side plot includes an example of temperature tendencies due to the model physics and the dynamics (cfSites data set of EC-EARTH, *amip* experiment, for details see section 3.2.2). The atmospheric column is divided into two regions: one including the BL and the shallow-cumulus cloud, and the one aloft. To distinguish between the two, we use the level of minimum Moist Static Energy (MSE). The definition of MSE entails that its minimum is located above the region where most water vapor is present.

Most of the fast physical processes involved in low-level cloud evolution are active below the level of minimum MSE. In the subcloud layer, the positive tendency due to turbulence and convection compensates the low-level advection of cold air, by redistributing warm near-surface air throughout the BL. Within the cloud layer, the negative temperature tendency due to the model physics results from the combined effect of condensation and radiative cooling. The tendency due to these physical processes counteracts the advection of warm air, resulting from the horizontal transport of air from the equator by the upper branch of the Hadley cell, and the subsidence of warm air from aloft.

Above the level of minimum MSE, the temperature tendency due to advection is compensated by the radiative tendency alone. In this region, the system is in a near RAE. As argued before, it is essential to ensure this balance in a SCM, otherwise the model solutions may drift. A complicating factor is that, in a SCM, the tendencies due to radiation and advection are estimated in different ways. While the radiative tendency depends on the atmospheric profile and is calculated interactively, in most SCMs the tendency associated with LS advection is prescribed as an external forcing. To obtain an approximate balance, one possibility is to scale the advective transport such that it matches the radiative tendency.

To explore this idea, a scaling factor λ_ϕ is introduced, where $\phi \in \{T, q_v\}$, with q_v the specific humidity. This scaling factor is calculated interactively through the following steps:

1. The SCM is driven by imposing the high-frequency dynamical tendency as in the GCM outputs;
2. The value of λ_ϕ is calculated as follows

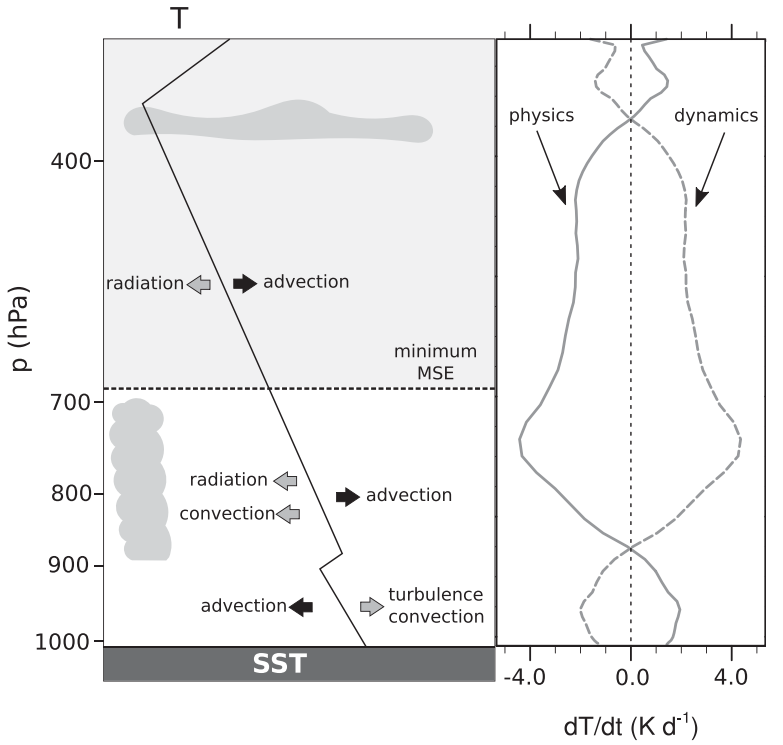

Figure 1. Schematic illustration of the physical processes involved in the temperature budget. The grey area indicates where a near RAE is found.

$$\lambda_\phi = \left| median_z \left(\left\langle \left. \frac{d\phi}{dt} \right|_{phys} (z,t) \right\rangle / \left\langle \left. \frac{d\phi}{dt} \right|_{dyn} (z,t) \right\rangle \right) \right| \tag{1}$$

where *phys* stands for model physics and *dyn* for dynamics, and the angle bracket indicates the mean;

3. The SCM is now forced by the scaled tendency, indicated by *RAE*, defined as follows

$$\left. \frac{d\phi}{dt} \right|_{RAE} (z,t) = \lambda_\phi \cdot \left. \frac{d\phi}{dt} \right|_{dyn} (z,t) \tag{2}$$

The steps 2 and 3 could be reiterated until λ_ϕ converges, but sensitivity studies demonstrate that one iteration is typically sufficient to ensure RAE (not shown). This study consists of sets of month-long SCM simulations. We assume that this period is long enough to obtain an approximate equilibrium for both T and q_v in the free troposphere, but also short enough to filter out seasonal dependences. Accordingly, λ_ϕ is calculated for each month separately.

3. Experimental Setup

3.1. Brief Description of EC-EARTH SCM

This study employs the SCM version of the atmospheric component of EC-EARTH. This is a state of the art GCM developed as a European joint effort on the basis of cycle 31r1 of the European Centre for Medium-range Weather Forecast (ECMWF) weather prediction model (Hazeleger et al., 2012; "IFS," 2006).

The BL clouds are represented through a suite of physical parameterizations. The vertical transport of heat and humidity across the BL is carried by both the turbulence and convection schemes. The former describes the exchange of heat and moisture with the surface and the subsequent vertical mixing in the clear and stratocumulus-topped BL using an Eddy-Diffusivity Mass-Flux approach (Köhler et al., 2011; Siebesma et al., 2007). The convection scheme describes the transport by shallow and deep cumulus clouds with a mass-flux approach based on Tiedtke (1989). Both parameterizations are coupled to a prognostic cloud scheme,

which predicts the cloud microphysical and precipitation properties (Tiedtke, 1993). Finally, the radiative fluxes are calculated on the basis of the atmospheric state profiles as described by Morcrette (1991).

3.2. Driving Data Sets

3.2.1. The ECMWF-fc Data Set

The first forcing data set, hereafter referred to as "ECMWF-fc", is based on a combination of analyses and short-range forecasts by the Integrated Forecasting System of the ECMWF (cycle 35r3–36r1). The standard output is used as archived in ECMWF's Meteorological Archival and Retrieval System (MARS). In MARS, the analysis fields are available at two timepoints per day, at 00 UTC and 12 UTC. These analysis fields are supplemented by 3 hourly output from two forecasts starting on these two analysis timepoints. Combining these analyses and forecasts yields a forcing data set for the SCM that has an effective time-resolution of 3 h.

3.2.2. cfSites Data Set

The second forcing data set is derived from the cfSites data archive (Webb et al., 2015), which is part of the Coupled Model Intercomparison Project 5 (CMIP5; Taylor et al., 2012). This data set consists of high-frequency point-sampling in some GCMs participating in CMIP5 at 120 selected grid points. The EC-EARTH GCM has outputs every three hours (i.e., once every three time steps) over the whole simulated period of the Atmospheric Model Intercomparison Project (AMIP), i.e., 1979–2008 (Gates, 1992). We use the data sets of the cfSites location 120, which is the closest to BCO. We consider the control experiment (*amip*) and the experiment corresponding to a homogeneous increase in SST by 4 K (*amip4K*).

3.3. SCM Experimental Setup

EC-EARTH SCM is driven by two different data sets, but using a consistent experimental setup. Since each data set comprises a slightly different ensemble of variables, the experimental setup needs to be designed such that it compensates for the lack of availability of some GCM variables, but still allows using both forcing data sets. The details of this setup are discussed in this section. Both data sets share a time-frequency of 3 h. At intermediate timepoints, the forcing and the thermodynamic state are linearly interpolated by the SCM.

3.3.1. LS Forcing Conditions

Various time-varying surface fields are provided to the SCM as boundary conditions. Both data sets include the SST and the surface pressure. The MARS archive also contains the roughness lengths for heat and momentum, the surface albedo, and the land sea mask. By contrast, for the cfSites data set, we use monthly mean data for these variables. Note that prescribing these surface properties allows the use of interactive surface fluxes, through the commonly used bulk closure technique of the surface exchange of heat and moisture.

The T and q_v tendencies associated with LS advective transport are prescribed (e.g., Siebesma et al., 2003; Vanzanten et al., 2011). For the ECMWF-fc forcing data set, the horizontal advective forcings are constructed from T and q_v fields as follows. First a $2^\circ \times 2^\circ$ three-dimensional subdomain centered near BCO (i.e., 13.6°N, 301.2°E) is extracted from the global data set. Successively, the advective tendencies in both horizontal directions are calculated at each grid point in the subdomain, using the centered difference method. Finally, the tendencies are horizontally averaged within a $0.5^\circ \times 0.5^\circ$gridbox around BCO. Vertical advective tendencies of T and q_v are calculated interactively by the SCM using a prescribed pressure velocity, also obtained from the MARS archive. In the cfSites data set, the vertical and horizontal components of the advective tendency are only available as a total. As a consequence, the cfSites SCM experiment uses a prescribed vertical advective tendency, and does not use interactive calculation based on the pressure velocity.

The zonal (u) and meridional (v) wind budgets are more tightly constrained compared to those of the thermodynamic variables. The LS advection of u and v is neglected, while the geostrophic wind velocity (u_g and $v_{g)}$ is assumed to be equal to the actual wind. This choice is motivated the lack of availability of both the LS advection and geostrophic wind in the cfSites data set. The impact of this limitation on the SCM results is considered a future research topic. A benefit of this simplification is that it allows focusing on the thermodynamic side of this problem, resulting in a more transparent analysis.

The λ scaling technique as described in section 2.3 is only applied to the 30 year cfSites experiments, and not to the ECMWF-fc experiment. The latter have the sole purpose of investigating if the SCM can reproduce the monthly mean budgets of T and $q_{v,}$ when provided with the best possible estimates of the boundary

conditions and forcings. If this is the case and no significant drift occurs, this creates confidence in the robustness of the SCM before using the more incomplete cfSites data set for a longer time period (30 years).

3.3.2. Initialization and Relaxation

The SCM is initialized with the vertical profiles of $\phi \in \{T, q_v, u, v\}$. During the simulation, the vertical profiles of ϕ are continuously relaxed toward the GCM state following the commonly used Newtonian method,

$$\left.\frac{d\phi}{dt}\right|_{rel} = -\frac{\phi - \phi_{GCM}}{\tau} \tag{3}$$

where the subscript *rel* indicates the tendency due to relaxation, ϕ_{GCM} the GCM outputs toward which the SCM results are relaxed, and τ the relaxation time scale, with a shorter τ implying a larger relaxation tendency. This time scale is height dependent, to allow the use of different relaxation intensities in different regions. Three types of relaxation are applied, and a schematic representation of the values of τ in the different regions of the atmosphere is shown in Figure 2. The sensitivity of the SCM setup to these relaxation time-scales is tested in Appendix C.

Relaxation is applied on T and q_v with $\tau_{TD} = 3$ h above the level minimum MSE, and $\tau_{TD} = 240$ h (10 days) below. This value of τ_{TD} allows the atmospheric layer with the largest amount of humidity and clouds to evolve freely, as the BL processes act on time scales shorter than 10 days. At the same time, the upper troposphere is more tightly constrained. Note that the level of minimum MSE is calculated interactively during the simulation; hence, it follows the evolution of the atmosphere.

The wind components, u and v, are relaxed toward the GCM profiles over the whole atmospheric column with $\tau_U = 3$ h. In the cfSites data set, u_g and v_g and the advection of wind are not available. The wind relaxation is designed to compensate for the lack of availability of these variables. Note that high-frequency variability in the wind forcing is ensured by the state used for relaxation.

The cloud fraction (CF), liquid water content (q_l), and ice water content (q_i) are relaxed above 400 hPa with $\tau_{CL} = 3$ h. This region is characterized by cirrus clouds, which are advected northward from the deep convective areas near the equator. The lateral advection of cloud properties, significant at these heights because of the long life-times of ice particles, is not available in both forcing data sets. The tight relaxation applied in this region is meant to mimic the effect of the LS advection of cloud particles. Their presence is important to ensure realistic radiative fluxes at the BL top. Consistently with the relaxation on the thermodynamic state, below 400 hPa we set $\tau_{CL} = 240$ h.

3.4. Details of the Simulations

Two sets of EC-EARTH SCM simulations at the BCO site are considered. The first is forced by the EC-EARTH-fc data set, and only covers the dry season of the year 2010. The second experiment employs the cfSites

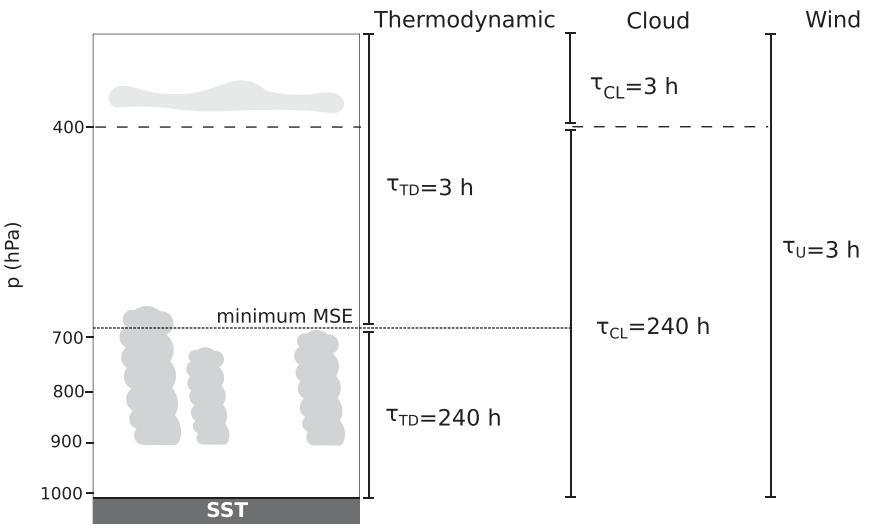

Figure 2. Schematic representation of the relaxation used in the experimental setup, with the employed time scales (τ).

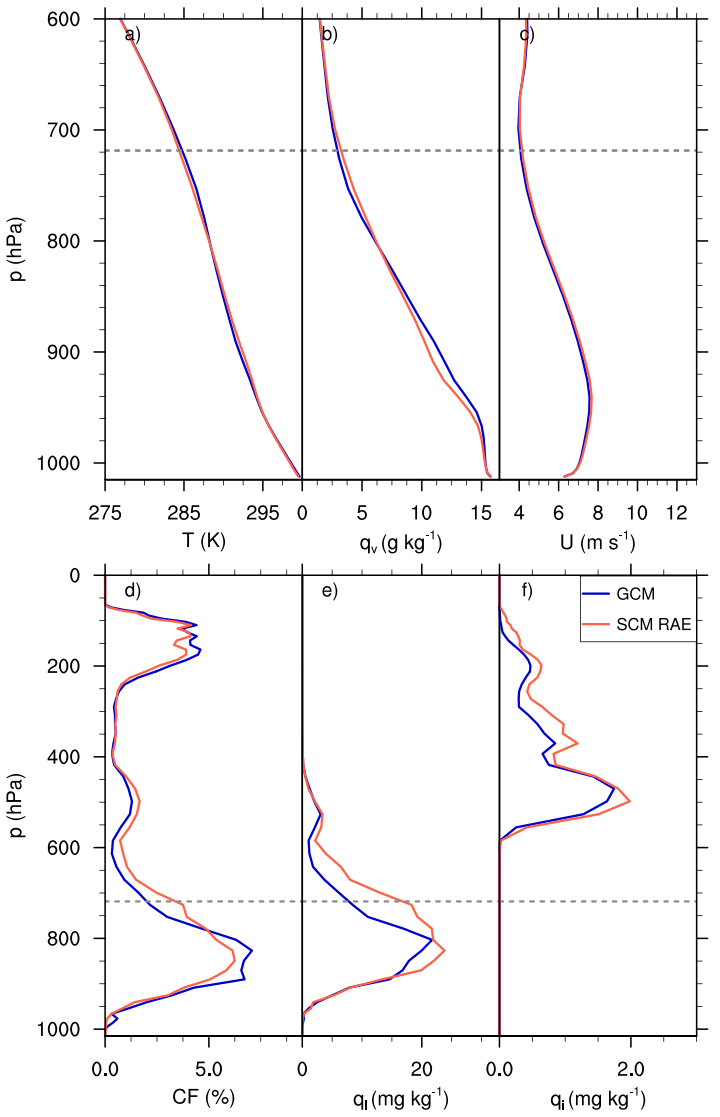

Figure 3. Mean profiles of the SCM results of ECMWF-fc experiment as compared to the forcing data set for (a) temperature (T), (b) water vapor content (q_v), (c) wind velocity (U), (d) cloud fraction (CF), (e) liquid water content (q_l), and (f) ice water content (q_i). The dashed line indicates the level of minimum MSE.

data set for driving the SCM, and covers 30 years of dry seasons in the time-period 1979–2008, for both the amip and amip4K experiments. As already argued, the ECMWF-fc simulations aim to create confidence in the skill of the SCM in reproducing GCM behavior, when provided with the best possible boundary conditions and forcings. By contrast, the cfSites simulations have the prime purpose of investigating if the response of low-level clouds in the Trades to an imposed climate perturbation as found in a GCM can be reproduced by a SCM, even with an incomplete forcing data set.

All experiments are deconstructed into series of month-long simulations, each initialized at the start of the month. Accordingly, each dry season consists of four simulations, each covering 1 month in the period from January to April. Consistent with the EC-EARTH GCM, the SCM simulations are performed with a time step of 1 h. The vertical grid consists of 91 levels for the ECMWF-fc experiment, and 62 levels for the cfSites experiment. This reflects the native grids of the associated GCM simulations from which the forcings were derived (more information about these vertical grids is available at www.ecmwf.int/en/forecasts/~documentation-and-support). In both discretizations, the lowest model level is at 10 m, and the vertical grid size gradually increases from 25 m to about 300 m at 3 km height. In total, there are 20 levels below 3 km, which roughly corresponds to the climatological height of the minimum MSE.

4. Results

4.1. ECMWF-fc Forcing

First, the SCM experiment using the ECMWF-fc forcing is discussed. The SCM results are compared to that of the forcing data set to assess to which extent they are consistent. In addition, budget analyses of various state variables are performed to provide more insight into the contribution of individual processes. The analysis focuses on time averages over the whole simulated period, which here corresponds to the dry season of 2010 (i.e., 4 months). Unless stated otherwise, all the results presented in the remainder of the article conform to this definition.

4.1.1. Thermodynamic and Cloud Structure

Figure 3 displays the vertical profiles of T, q_v and the total horizontal wind, U, as well as the vertical cloud structure, i.e., CF, q_l and q_i. The overall BL state is reproduced by the SCM to a satisfactory degree (Figures 3a–3c). The wind velocity is rather constrained by construction, while the thermodynamic state is influenced by the relaxation mostly below the level of minimum MSE, indicated by the grey dashed line. As a result, the only noticeable differences in T and q_v are at the inversion, with a slightly more pronounced stratification in the SCM (Figures 3a and 3b). Furthermore, the SCM presents a consistent cloud structure with the ECMWF-fc data sets. The profiles show the majority of clouds below the level of minimum MSE, with a second and minor peak in the upper troposphere (150 hPa), corresponding to cirrus clouds. We speculate that the small differences in cloud structure are likely due to the different versions of the cloud scheme used in the SCM and in the GCM. Nevertheless, the good agreement in cloud structure is remarkable and not trivial, considering that the physics in the lower atmosphere is completely free to act.

4.1.2. Illustration of the RAE Method

The thermodynamic and cloud structures are the combined result of the effect of dynamics, physics and relaxation. To assess what is the contribution of each of these tendencies, Figures 4a and 4b show a breakdown of the budgets of temperature and humidity into the dynamical, physical and relaxation components.

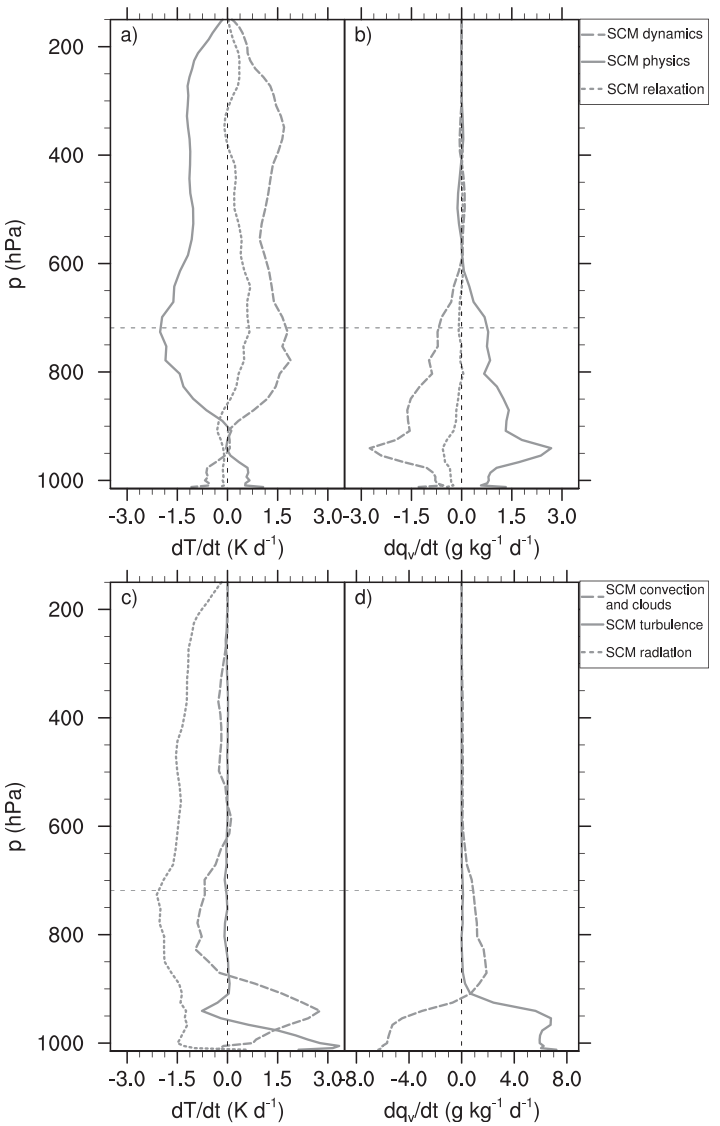

Figure 4. The tendency due to model physics, LS advection and relaxation for the ECMWF-fc experiment for (a) temperature budget and (b) humidity budget. The different components of the tendency due to model physics for (c) temperature budget, and (d) humidity budget. The dashed line indicates the level of minimum MSE.

Figures 4c and 4d show a more detailed breakdown of the physics tendency into the contributions of the SCM parameterizations. Note that the convection and cloud scheme are combined into one contribution.

Throughout the column, a near equilibrium exists between the physical and dynamical tendencies. The contribution of the relaxation is of only secondary importance (Figures 4a and 4b). While this experiment is not scaled using the RAE method, it is still possible to calculate the λ factors associated with these budgets. This yields a λ_T ranging between 0.92 and 1.06 for the individual months, and a λ_q varying between 0.83 and 0.97. Therefore, a near equilibrium is achieved in these preliminary runs, without a large contribution coming from the relaxation. The SCM physics is indeed capable of compensating a GCM forcing to a reasonable degree, even when running freely and with prescribed forcing which includes high-frequency variations. This result gives confidence that the SCM is representative of the forcing GCM at this location.

As discussed in section 2.3, most of the fast physics is active below the level of minimum MSE (dashed line in Figure 4). Above this level, the temperature tendency due to physics is almost completely determined by its radiative component (Figure 4c). We hence conclude that the level of minimum MSE is a good threshold for identifying the region where the atmosphere is in near RAE. Below the level of minimum MSE, the temperature and humidity tendency due to physics include a considerable contribution coming from the turbulence and, in combination, convection and clouds (Figures 4c and 4d). Turbulence acts primarily close to the surface, and vertically redistributes warm and humid near-surface air throughout the BL. Convection and clouds contribute to the budgets by transporting warm and humid air higher up in the cloud layer. In addition, the cloud scheme affects the temperature budget by latent heat effects. All these tendencies are always much larger than the relaxation tendency within this height range. We therefore conclude that the low-level physics in the SCM acts freely.

4.2. cfSites Forcing: Current Climate

The results presented in section 4.1 are promising. However, the ECMWF-fc data set, although very complete, does not include future climate conditions. Since the main goal of this study is to explore a possible SCM framework for low-cloud feedback studies, the next step is to use the cfSites data set to this purpose. An advantage is that the SCM physics is exactly the same as in the EC-EARTH GCM. This creates an opportunity for exploring both the advantages and limitations of the proposed method.

4.2.1. Benefits of the λ Scaling

First, the cfSites-amip experiment, reflecting current climate, is considered. The SCM results reflect means over 30 years of dry seasons near BCO. Similar to the ECMWF-fc experiments, the same high-frequency time-variation in the forcing is maintained. Surprisingly, the preliminary experiment yields an average value of $\lambda_T = 0.54$, varying between 0.37 and 0.97. The corresponding mean $\lambda_q = 0.76$, ranging between 0.35 and 1.06. These values imply that the SCM physics does not fully counteract the dynamics, and that relaxation plays a key role in the budgets. After performing the RAE scaling and rerunning the experiment, the mean temperature and humidity tendencies due to advection and physics are balanced, and the relaxation is of secondary importance in the budget. This is shown in Figure 5. This budget is qualitatively and quantitatively consistent with that of the ECMWF-fc experiment discussed in the previous section (Figures 4a and 4b).

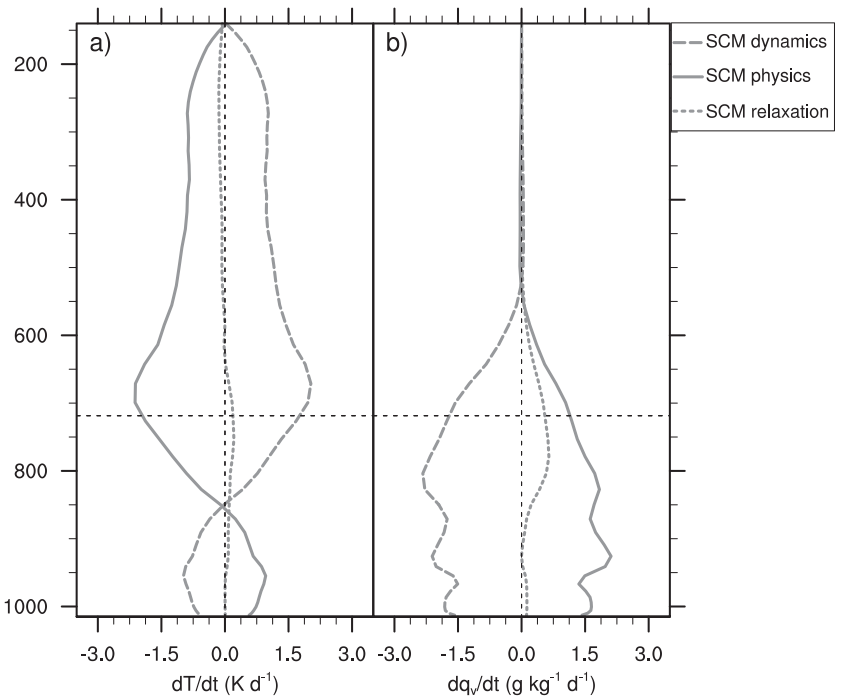

Figure 5. Same as Figure 4 but for the experiment exploiting the cfSites data set.

We speculate that the initial mismatch between the imposed advective tendency and the physical tendency in the cfSites experiment has two possible causes. Firstly, the setup of the cfSites experiment is further idealized with respect to the ECMWF-fc experiment, mainly to deal with the lack of availability of separate vertical and horizontal components of the advective tendency. The results might suffer from this simplification. However, a sensitivity test, using a reconstructed vertical advection based on the pressure velocity, does not show a reduced discrepancy between dynamics and physics (not shown). This result makes this aspect unlikely to be the cause. Secondly, the advective tendency in the EC-EARTH cfSites data set might be affected by a miscalculation. Proving this hypothesis would require rerunning the GCM climate simulations, which is far beyond the scope of this study and the means of the authors. However, follow-up studies are indeed recommended for shedding light on this issue.

The agreement between the ECMWF-fc SCM experiment and the forcing GCM in terms of the temperature budget supports the robustness of the SCM physics. In addition, the RAE-scaled cfSites experiment performs equally well in terms of balancing the advective forcing. Accordingly, this justifies adopting the working hypothesis that the λ-scaling is a promising method for dealing with forcing data sets that yield an initial mismatch between dynamics and physics, and it provides a way to work with incomplete forcing data sets. One aim of this study is to gain more insight into this possibility. If successful, the RAE method can be used to drive an arbitrary SCM with forcings from different GCMs. This research can also lead to a better understanding of which GCM output is essential for driving a SCM for multiyear experiments.

4.2.2. Thermodynamic and Cloud Structure

Similar to section 4.1, we investigate to what extent the SCM cfSites experiment is representative of the BL and cloud structure of EC-EARTH GCM. Figure 3 displays the vertical profiles of T, q_v, U, CF, q_l and q_i, for EC-EARTH GCM and the SCM experiment. The overall thermodynamic state is well captured by the SCM, although the SCM thermodynamic conditions are slightly colder and drier with respect to the GCM (Figures 3a and 3b). Moreover, the inversion stratification is less noticeable, probably because of the lack of an interactive subsidence. Also the wind velocity is still reasonably well captured by the SCM (Figure 3c). A slight underestimation in amplitude is found near the surface, which might be explained by the further idealization of the surface conditions in this experiment with respect to the ECMWF-fc experiment (section 3.3.1). A weaker wind contributes to the differences in the thermodynamic state in the subcloud layer through the bulk closure of the surface fluxes. Despite the small differences in the BL structure between the SCM and

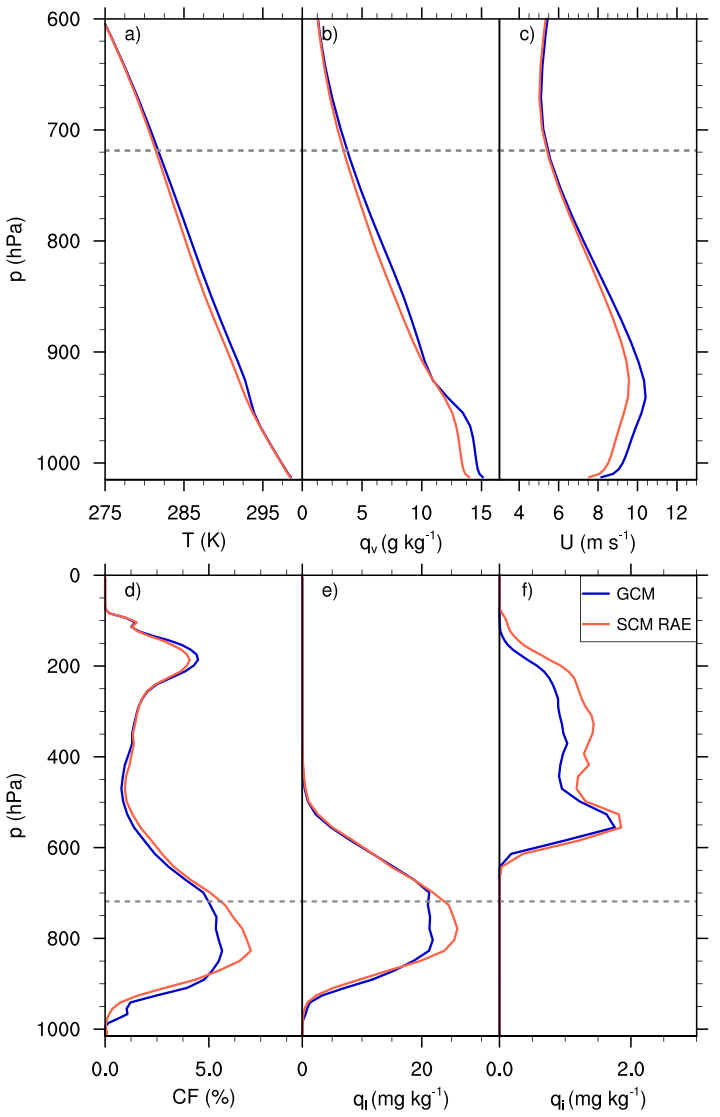

Figure 6. Same as Figure 3 but for the cfSites experiment.

GCM results, the cloud structure found in the GCM results is well reproduced by the SCM (Figures 6a–6c). The better agreement in cloud structure in this experiment with respect to the ECMWF-fc experiment suggests that in the latter the differences are caused by slight differences in the model physics, and not by the experiment setup.

4.2.3. Representation of the High-Frequency Variability

The cloud structure discussed previously is the result of 30 years integration, which includes all the "weather" fluctuations. As an illustration of the cloud variability within 1 month, Figure 7 shows the time dependency of CF for April 1996 for both the GCM and the SCM. The low-level cloud structure in the GCM presents a distinct diurnal cycle and noticeable variations in the cloud layer depth (Figure 7a). All these features are qualitatively captured by the SCM results, although minor differences do occur (Figure 7b). We speculate that these differences reflect SCM numerical artifacts, such as grid locking (Lenderink & Holtslag, 2000). This SCM issue is defined as the situation in which the BL cannot descend because of numerical entrainment. This results in local overestimations of CF. However, the high-frequency variation in the forcing quickly "unlock" these situations. As a result, the time-variation of the low-level clouds is well captured.

To gain insight into this agreement, we systematically analyze 30 years of monthly and daily means of vertically integrated cloud properties, including the total cloud cover (TCC), the liquid water path (LWP), and the ice water path (IWP). Figure 8 displays the SCM results against the GCM ones for these variables, and each plot reports the correlation coefficient for the daily means ($r_{d)}$ and for the monthly means ($r_{m)}$. This coefficient gives an indication of how much the SCM represents the variability of the GCM outputs. If the results corresponded perfectly, all the points would lie on the diagonal (black line), and the correlation coefficient would be 1. The less representative the SCM results become, the more noticeable the spread of the points is, and the correlation coefficient approaches 0.

Overall, the SCM is representative of the variability found in the cfSites data set over the two time scales considered, with a small improvement in the correlations of monthly means. The quantity that is captured best is the IWP (Figure 8c). This result partly reflects the tight cloud relaxation above 400 hPa, where most of the cloud ice is located. The correlation of TCC is also partially influenced by the high-level clouds, while LWP reflects the short-time variability of the low-level clouds alone. Similar to what discussed for Figure 7, the low-level cloud variability might be affected by grid locking as well as slight misrepresentation in the case of deeper convective events, that results in a nonsystematic LWP overestimation. This causes a larger spread in the SCM daily of monthly means with respect to that of the GCM, which reduces the correlation coefficient. However, such a correlation coefficient as found for LWP is high enough to point at good skills of the SCM in reproducing the short-time variability of BL clouds of the forcing GCM.

4.3. cfSites Forcing: Response to SST Warming

The previous analysis demonstrates that using the RAE method gives SCM results that are representative of the forcing data set. In this section, we investigate whether the RAE method is also applicable in low-cloud feedback studies. To this end, we use the cfSites data set, this time using forcings derived from amip4K experiment.

The configuration of the cfSites amip4K experiment is the same as that for current climate (section 3.3). The λ values are calculated based on preliminary runs, and then used to scale the dynamical tendencies, after

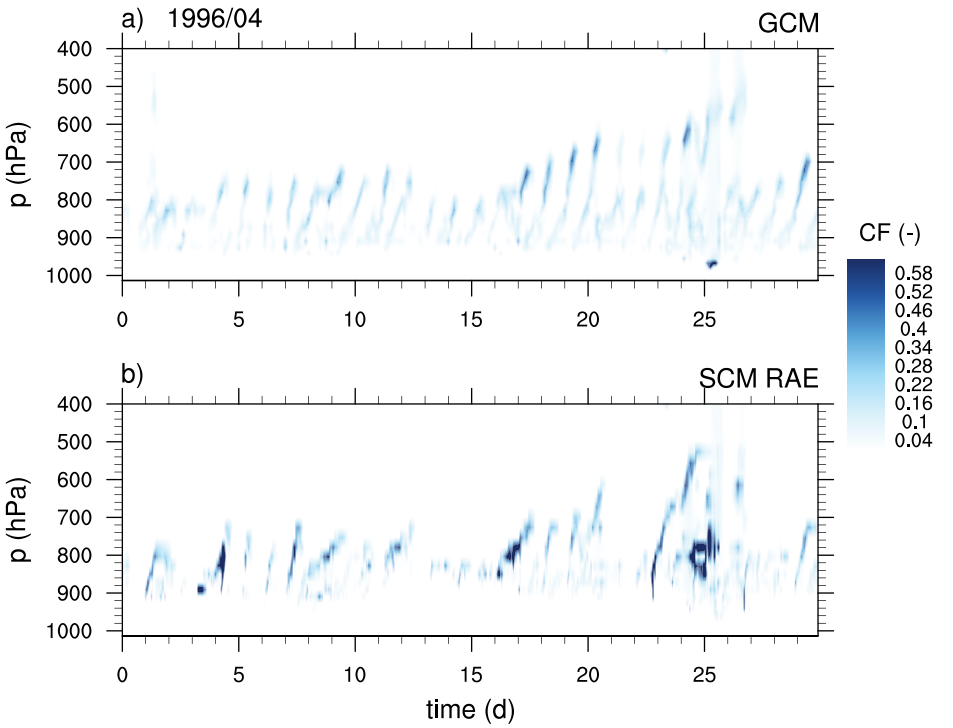

Figure 7. Illustration of the variability within April 1996 of the cloud fraction (CF) for (a) EC-EARTH GCM results as stored in the cfSites archive and (b) SCM RAE experiment.

which the experiment is repeated. The scaling parameters for amip4K are similar to those of the amip experiment: the average value of $\lambda_T = 0.51$, varying between 0.45 and 0.95, while the mean $\lambda_q = 0.72$, ranging from 0.30 to 1.16. Also in this case, the RAE scaling yields SCM experiments that achieve an approximate equilibrium, with only a minor contribution coming from the relaxation.

4.3.1. Estimate of the Cloud Response

This section focuses on the response to a homogeneous warming of SST, defined as the difference between the mean state in amip4K and in amip experiment, and indicated by Δ. Figure 9 presents the profiles of ΔCF, Δq_l, and Δq_i for the GCM and the SCM results.

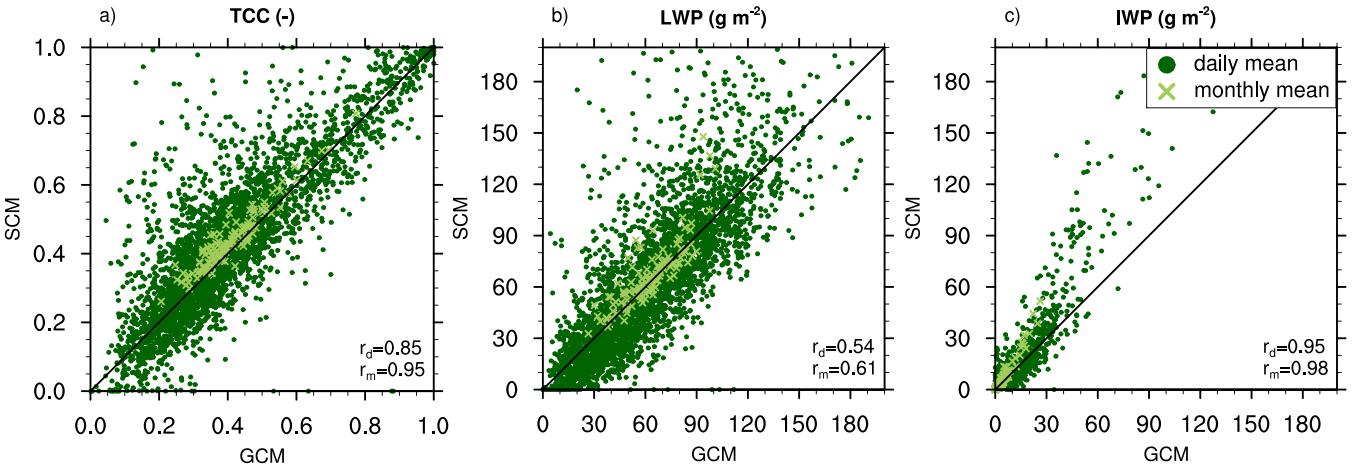

Figure 8. Scatterplot of the GCM results against the SCM ones of the daily and monthly means of (a) TCC, (b) LWP, and (c) IWP. Each plot includes the correlation coefficients of the daily means (r_d), and of the monthly means (r_m).

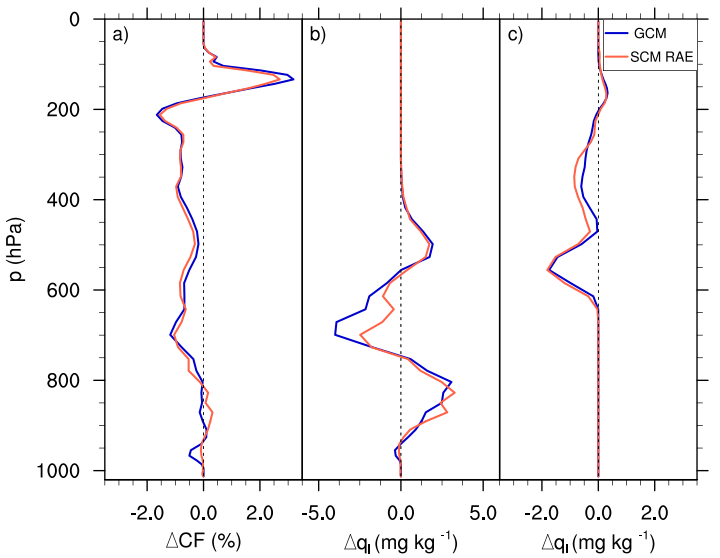

Figure 9. Response to a SST increase of 4 K in (a) cloud fraction (ΔCF), (b) liquid water content (Δq_l), and (c) ice water content (Δq_i).

The cloud response in EC-EARTH GCM is a combination of mechanisms all apparent in Figure 9. First, the deepening of the troposphere results in a double peak in the ΔCF profile between 100 and 300 hPa (Figure 9a). The Fixed Anvil Temperature (FAT) hypothesis states that the tropopause temperature is expected to remain constant, hence in a warmer climate the high-level cloud top raises (Hartmann & Larson, 2002). Below that, CF reduces throughout the atmospheric column. Furthermore, the increased elevation of the freezing level is noticeable between 400 and 500 hPa, as part of q_i is replaced by q_l (Figures 9b and 9c). Below the freezing level, q_l profile shows a decrease topped by an increase (Figure 9b).

The SCM results reproduce all the previously described changes in the cloud structure remarkably well. The FAT is reproduced by the SCM, as well as the reduction in q_i. These changes are partly affected by the cloud relaxation in the upper atmosphere. However, also the shift in freezing level is reproduced, and likewise for the response of the low clouds. The latter is particularly far from trivial, as it is completely carried by free physics. More specifically, both the positive and negative peaks in q_l and the CF response are reproduced well.

The response in the cloud vertical structure directly impacts the radiative budget. This impact is known as the *cloud feedback*. Following previous studies (e.g., Cess et al., 1989; Zhang et al., 2013), we use a proxy for the cloud feedback, defined as the difference in the cloud radiative effect (CRE) between amip4K and amip results normalized by the SST increase. CRE is defined as the difference between the net downward top-of-atmosphere radiative flux in all-sky and clear-sky conditions. It has been shown that a correlation exists between ΔCRE/ΔSST and the actual cloud feedback (Soden et al., 2004), hence hereafter the two definitions are used as approximate synonyms.

Both the upper shift in the high-level clouds and the reduction in the mid- and low-level clouds lead to a positive cloud feedback. The value of ΔCRE/ΔSST for EC-EARTH GCM is 1.30 W m^{-2} K^{-1}, while the SCM experiment yields a cloud feedback of 0.87 W m^{-2} K^{-1}. These results suggest that the SCM cloud feedback is representative of the parent GCM. It is worth stressing that the relaxation tendencies are negligibly small compared to the physics components in both amip and amip4K. Therefore, the response of the model physics to the changes in the LS conditions is not constrained by relaxation.

4.3.2. Robustness of the Cloud Feedback

The previous results could depend on the particular sample of considered months. To investigate this, we consider averages over subsets of randomly selected months. For a full description of the calculation of the average and the standard deviation (σ) over an ensemble of subsets, we refer to the Appendix A.

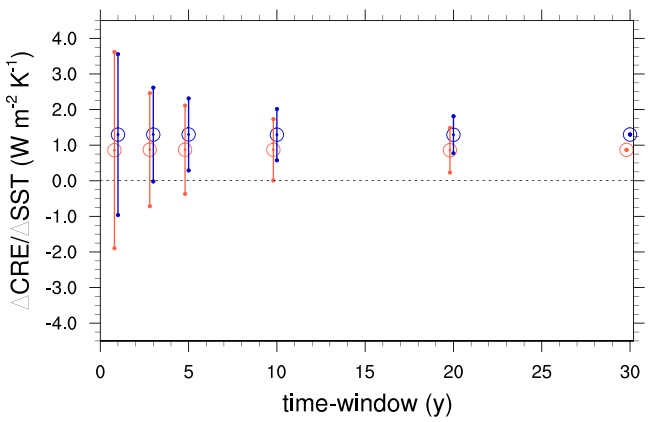

Figure 10. Average value and 2 standard deviations of ΔCRE/ΔSST for the whole simulated period and for subsets composed of randomly selected months. Consistent with Figure 9, the GCM results are in blue and the SCM ones in red.

Figure 10 presents $\frac{\overline{\Delta CRE}}{\Delta SST}$ as a function of the *time-window*, which is defined as the total simulated period and varies in $\{1, 2, 5, 20, 30\}$ years. Note that, since our study includes only the dry season, a time-window of 1 year corresponds to 4 months of simulation. Figure 10 also shows the variability within each ensemble of subsets, calculated as twice the standard deviation.

In Figure 10, the GCM results for a 20 year time-window present a variability which is small as compared to the inter-model spread found in previous studies (e.g., Brient et al., 2016; Zhang et al., 2013). For shorter time-windows, the variability in the GCM results becomes larger, but even at 5 years the sign of the feedback is still statistically significant.

The mean values of ΔCRE/ΔSST for the SCM experiment are always representative of the GCM outputs, as they are situated within the range of uncertainty of the GCM. The variability of the SCM results are

larger than the one of the GCM results. For a time-window shorter than 10 years, there might be ambiguity on the sign of the feedback in the SCM results, which is not found for the GCM. In conclusion, this analysis confirms that the estimated cloud feedback is a robust signal, and is not affected by the selected period, for both GCM and SCM results.

5. Discussion and Conclusions

This study explores and evaluates a new method for exploiting existing high-frequency output data sets to drive SCMs. The EC-EARTH SCM is driven by the LS forcing conditions near BCO as derived from the ECMWF-fc and the cfSites data set. The dry season at this location is representative of the Trades, where the free troposphere is in a near RAE. This near balance is effectively ensured in the SCM by scaling the monthly mean advective tendency of temperature and humidity. To this end, the scaling factor λ is defined and calculated on a monthly basis. As a result, the relaxation tendency becomes negligible in the thermodynamic budgets, leaving the BL physics free. In addition, the natural high-frequency variability in the GCM-derived forcing is retained.

By using the RAE method, we report a satisfactory agreement between SCM and GCM, both in current climate and in the response to a climate perturbation. For current climate, the BL thermodynamic state and the cloud amount and structure are reproduced. Furthermore, SCM clouds respond to future climate in a representative way of the forcing GCM, in terms of changes in cloud amount and structure, and in the positive sign of the cloud feedback. These results suggest that the RAE framework is an effective way to perform SCM studies in general, for testing physical parameterizations in a controlled setting but also for gaining understanding in the role of parameterized physics in the low-level cloud feedback. Moreover, the method proves efficient in dealing with forcing data sets that do not initially yield a near equilibrium between dynamics and physics. This can be due to incomplete forcing data, but also to inconsistencies between the physics of the SCM and the GCM. This implies that, by using the RAE method, one can drive an arbitrary SCM with outputs from any other GCM. The only necessary conditions are the availability of the relevant GCM outputs at high frequency, and the applicability of RAE, which holds for specific meteorological conditions such as in the Trades.

One of the main novelties of this SCM setup is that it retains the natural high-frequency variability in the LS forcing. Previous SCM intercomparison studies, focusing on the cloud-climate feedback, have predominantly limited their analyses to steady states (Dal Gesso et al., 2015b; Zhang et al., 2013). Consistent with the results reported by Brient and Bony (2012), this study suggests that considering steady states for representing the whole complexity of the climate system is too idealized. The main advantage of this approach is that it preserves the subdiurnal signal as appears in the GCM, which eliminates the necessity to introduce artificial reconstructions of this variability.

In line with previous studies (Neggers, 2015; Nuijens et al., 2015; Webb et al., 2015), this article highlights the opportunities created by data sets like that of the cfSites initiative. For applying the RAE method, some specific variables are indeed fundamental, others would improve the experimental setup by reducing the assumptions and simplifications needed. Although the availability of these variables can depend on many aspects, we take the opportunity to list all the LS forcing conditions necessary for this setup in Appendix B.

In conclusion, the experimental SCM setup explored in this study enables us to exploit the cfSites data set to directly drive one SCM with its parent GCM. The opportunity of driving one SCM with several GCM outputs is currently being explored in a companion study by the authors. This follow-up article will investigate whether the BL cloud response to climate change is mainly controlled by the model physics or by the LS dynamics. Such a study might shed new light on the mechanisms at the basis of the BL cloud-climate feedback in GCMs.

Appendix A: Definitions of the Subset Statistics

The mean cloud feedback of an arbitrary subset k, which contains N months in total, is

$$\left.\frac{\Delta \mathrm{CRE}}{\Delta \mathrm{SST}}\right|_k = \frac{1}{\Delta \mathrm{SST}}\left[\frac{1}{N}\sum_{n=1}^{N}\mathrm{CRE}\Big|_{\mathrm{amip4K}}(r(n)) - \frac{1}{N}\sum_{n=1}^{N}\mathrm{CRE}\Big|_{\mathrm{amip}}(r(n))\right] \tag{A1}$$

where $r(n)$ is a random number, which varies between 1 and 120 and identifies one of the considered months, with 1 corresponding to January 1979 and 120 to April 2008. The average, indicated by the

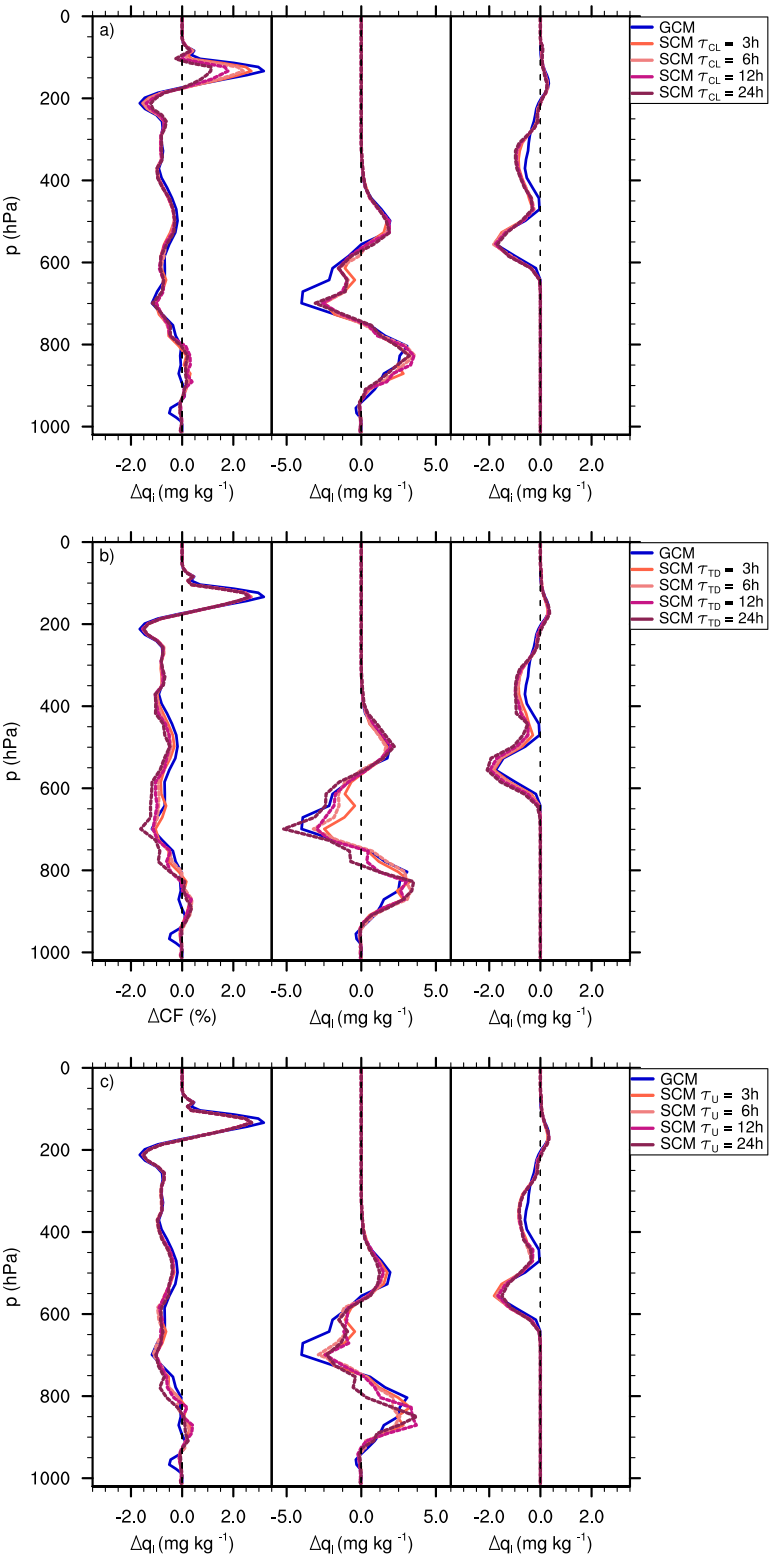

Figure C1. Mean profiles of Δfof Δf_i, and Δn_i. Each plot includes the mean profiles obtained by using the cfSites outputs of the EC-EARTH GCM and the results of the SCM RAE experiment with four different relaxation time scales. Figure C1a explores the effect of τ_{CL}, Figure C1b of τ_{TD} and Figure C1c of τ_{U}.

overbar, and the standard deviation, indicated by σ, over the whole group of subsets with a total of N months are defined as

$$\overline{\frac{\Delta CRE}{\Delta SST}}(N) = \frac{1}{K}\sum_{k=1}^{K}\left.\frac{\Delta CRE}{\Delta SST}\right|_k \tag{A2}$$

$$\sigma(N) = \sqrt{\frac{1}{K}\sum_{k=1}^{K}\left(\left.\frac{\Delta CRE}{\Delta SST}\right|_k - \overline{\frac{\Delta CRE}{\Delta SST}}(N)\right)^2} \tag{A3}$$

where $K = 100{,}000$ is the total number of subsets. Convergence tests on K indicate that this value ensures that the results do not depend on the selected months. Since our study includes only the dry season, a group of 4 months is interpreted as 1 year of simulation. We define the *time-window* as the considered N values in years of simulations, hence it varies in $\{1, 2, 5, 20, 30\}$ years.

Appendix B: List of Fundamental Variables

A complete list of all of the LS forcing conditions necessary for this setup follows:

- the advective tendencies of temperature and humidity, possibly with the vertical and horizontal components separated;
- the advective tendencies of cloud properties;
- the advection of the wind velocity and the geostrophic wind components;
- the surface properties.

Appendix C: Sensitivity to Relaxation Time Scales

In this section, we explore the sensitivity of the cloud feedback to the different relaxation time scales in the region of the atmosphere which is more tightly relaxed. In the present experimental setup, these time scales are all set equal to 3 h (Figure 2). Each of the employed relaxation time scales is now changed and set equal to 6, 12, or 24 h. In the following analysis, we address the effect of applying these relaxations on the estimated cloud feedback.

Figure C1a shows the effect of the relaxation on the high-level clouds. The profiles of ΔCF, Δq_l, and Δq_i are displayed for all the considered τ_{CL}. The profiles differ especially in ΔCF above 200 hPa. With a τ_{CL} of 24 h, the increase in CF at around 150 hPa in the future climate is still noticeable but reduced. Smaller differences are present also below 400 hPa, because of the variation in the radiative fluxes caused by the different cloud structure above. However, the mid- and low-level clouds are very consistent among all the experiments.

The effect of the relaxation of the thermodynamic state above the level of minimum MSE is assessed in Figure C1b. The impact of τ_{TD} on ΔCF, Δq_l, and Δq_i profiles is more noticeable with respect to Figure C1a, especially between 600 and 800 hPa. With a larger τ_{TD}, the warming of this atmospheric region in the amip4K experiment is more effective. This results in a more pronounced reduction of the mid-level clouds.

Lastly, we investigate the effect of τ_U, and the results of this sensitivity study are collected in Figure C1c. In this case, the wind becomes weaker for a longer relaxation time scale (not shown). The reduction of the wind results in a weakening of the surface fluxes, and in a downward shift of the low-level clouds (Nuijens & Stevens, 2012). As a result, the region in which q_l increases is shallower for a longer τ_U.

To summarize these results, we report in Table C1 the values of $\Delta CRE/\Delta SST$ calculated for each sensitivity study. All the estimated cloud feedbacks are positive, and the variability is limited with respect to

Table C1
Values of ΔCRE/ΔSST Calculated for the Different Sensitivity Studies

	$\Delta CRE/\Delta SST$ (W m^{-2} K^{-1})			
τ (h)	3	6	12	24
τ_{CL}	0.87	0.80	0.83	0.83
τ_{TD}	0.87	0.82	1.00	1.14
τ_U	0.87	0.79	0.79	0.89

the range of cloud feedbacks reported in previous SCM multimodel studies (Dal Gesso et al., 2015b; Zhang et al., 2013). We conclude that the effect of the employed relaxations does not strongly affect the estimated cloud-climate feedback.

Acknowledgments
The research leading to this article has received funding from the project "Energy Transitions and Climate Change" of the "Excellence Initiative" of the University of Cologne. The authors are very grateful to Frank Selten for providing them with the EC-EARTH GCM outputs and for helping with setting the details of the SCM physics such that it is completely consistent with the host GCM. The authors want to take the opportunity to thank Stephanie Reilly for proof-reading the manuscript. The authors would also like to acknowledge the Editor and two anonymous reviewers for their constructive comments, which improve a lot the quality of the manuscript. The SCM and GCM results can be downloaded from the repository http://gop.meteo.uni-koeln.de/simneggers/DalGesso-Neggers2018_James.

References

Blossey, P. N., Bretherton, C. S., Zhang, M., Cheng, A., Endo, S., Heus, T., . . . Xu, K.-M. (2013). Marine low cloud sensitivity to an idealized climate change: The CGILS LES intercomparison. *Journal of Advances in Modeling Earth Systems*, *5*, 234–258. https://doi.org/10.1002/jame.20025

Bony, S., & Dufresne, J.-L. (2005). Marine boundary layer clouds at the heart of tropical cloud feedback uncertainties in climate models. *Geophysical Research Letters*, *32*, L20806. https://doi.org/10.1029/2005GL023851

Brient, F., & Bony, S. (2012). Interpretation of the positive low-cloud feedback predicted by a climate model under global warming. *Climate Dynamics*, *40*, 2415–2431.

Brient, F., Schneider, T., Tan, Z., Bony, S., Qu, X., & Hall, A. (2016). Shallowness of tropical low clouds as a predictor of climate models' response to warming. *Climate Dynamics*, *47*(1–2), 433–449.

Brueck, M., Nuijens, L., & Stevens, B. (2015). On the seasonal and synoptic time-scale variability of the north atlantic trade wind region and its low-level clouds. *Journal of the Atmospheric Sciences*, *72*(4), 1428–1446.

Cess, R. D., Potter, G. L., Blanchet, J. P., Boer, G. J., Ghan, S. J., Kiehl, J. T., Yagai, I. (1989). Interpretation of cloud-climate feedback as produced by 14 atmospheric general circulation models. *Science*, *245*(4917), 513–516.

Cronin, T. W., & Jansen, M. F. (2016). Analytic radiative-advective equilibrium as a model for high-latitude climate. *Geophysical Research Letters*, *43*, 449–457. https://doi.org/10.1002/2015GL067172

Dal Gesso, S., Siebesma, A. P., & de Roode, R. S. (2015a). Evaluation of low-cloud climate feedback through single-column model equilibrium states. *Quarterly Journal of the Royal Meteorological Society*, *141*(688), 819–832.

Dal Gesso, S., Siebesma, A. P., de Roode, R. S., & van Wessem, J. M. (2014). A mixed-layer model perspective on stratocumulus steady-states in a perturbed climate. *Quarterly Journal of the Royal Meteorological Society*, *140*(684), 2119–2131.

Dal Gesso, S., van der Dussen, J. J., Siebesma, A. P., de Roode, S. R., Boutle, I. A., Kamae, Y., Vial, J. (2015b). A single-column model intercomparison on the stratocumulus representation in present-day and future climate. *Journal of Advances in Modeling Earth Systems*, *7*, 617–647. https://doi.org/10.1002/2014MS000377

Gates, W. L. (1992). AMIP: The atmospheric model intercomparison project. *Bulletin of the American Meteorological Society*, *73*(12), 1962–1970.

Hartmann, D. L., & Larson, K. (2002). An important constraint on tropical cloud—Climate feedback. *Geophysical Research Letters*, *29*(20), 1951. https://doi.org/10.1029/2002GL015835

Hartmann, D. L., Ockert-Bell, M. E., & Michelsen, M. L. (1992). The effect of cloud type on earth's energy balance: Global analysis. *Journal of Climate*, *5*(11), 1281–1304.

Hazeleger, W., Wang, X., Severijns, C., Ştefănescu, S., Bintanja, R., Sterl, A., van der Wiel, K. (2012). EC-Earth V2. 2: Description and validation of a new seamless earth system prediction model. *Climate Dynamics*, *39*(11), 2611–2629.

IFS documentation—Cy31r1: Physical processes. (2006). Reading, UK: ECMWF.

Köhler, M., Ahlgrimm, M., & Beljaars, A. (2011). Unified treatment of dry convective and stratocumulus-topped boundary layers in the ecmwf model. *Quarterly Journal of the Royal Meteorological Society*, *137*(654), 43–57.

Lenderink, G., & Holtslag, A. A. M. (2000). Evaluation of the kinetic energy approach for modeling turbulent fluxes in stratocumulus. *Monthly Weather Review*, *128*(1), 244–258.

Medeiros, B., & Nuijens, L. (2016). Clouds at barbados are representative of clouds across the trade wind regions in observations and climate models. *Proceedings of the National Academy of Sciences of the United States of America*, *113*(22), E3062–E3070.

Morcrette, J.-J. (1991). Radiation and cloud radiative properties in the European Centre for Medium Range Weather Forecasts forecasting system. *Journal of Geophysical Research*, *96*, 9121–9132.

Nam, C., Bony, S., Dufresne, J.-L., & Chepfer, H. (2012). The 'too few, too bright' tropical low-cloud problem in CMIP5 models. *Geophysical Research Letters*, *39*, L21801. https://doi.org/10.1029/2012GL053421

Neggers, R. (2015). Attributing the behavior of low-level clouds in large-scale models to subgrid-scale parameterizations. *Journal of Advances in Modeling Earth Systems*, *7*, 2029–2043. https://doi.org/10.1002/2015MS000503

Nitta, T., & Esbensen, S. (1974). Heat and moisture budget analyses using bomex data. *Monthly Weather Review*, *102*(1), 17–28.

Nuijens, L., Medeiros, B., Sandu, I., & Ahlgrimm, M. (2015). The behavior of trade-wind cloudiness in observations and models: The major cloud components and their variability. *Journal of Advances in Modeling Earth Systems*, *7*, 600–616. https://doi.org/10.1002/2014MS000390

Nuijens, L., Serikov, I., Hirsch, L., Lonitz, K., & Stevens, B. (2014). The distribution and variability of low-level cloud in the north atlantic trades. *Quarterly Journal of the Royal Meteorological Society*, *140*(684), 2364–2374.

Nuijens, L., & Stevens, B. (2012). The influence of wind speed on shallow marine cumulus convection. *Journal of the Atmospheric Sciences*, *69*(1), 168–184.

Rauber, R., Ochs, H. T., III, Di Girolamo, L., Göke, S., Snodgrass, E., Stevens, B., Twohy, C. H. (2007). Rain in shallow cumulus over the ocean: The RICO campaign. *Bulletin of the American Meteorological Society*, *88*(12), 1912–1928.

Ruppert, J. (2016). Diurnal timescale feedbacks in the tropical cumulus regime. *Journal of Advances in Modeling Earth Systems*, *8*, 1483–1500. https://doi.org/10.1002/2016MS000713

Siebesma, A., Bretherton, C., Brown, A., Chlond, A., Cuxart, J., Duynkerke, P., Stevens, D. E. (2003). A large eddy simulation intercomparison study of shallow cumulus convection. *Journal of the Atmospheric Sciences*, *60*(10), 1201–1219.

Siebesma, A. P., & Cuijpers, J. W. M. (1995). Evaluation of parametric assumptions for shallow cumulus convection. *Journal of the Atmospheric Sciences*, *52*(6), 650–666.

Siebesma, A. P., Soares, P. M. M., & Teixeira, J. (2007). A combined eddy-diffusivity mass-flux approach for the convective boundary layer. *Journal of the Atmospheric Sciences*, *64*(4), 1230–1248.

Sobel, A., Bellon, G., & Bacmeister, J. (2007). Multiple equilibria in a single-column model of the tropical atmosphere. *Geophysical Research Letters*, *34*, L22804. https://doi.org/10.1029/2007GL031320

Soden, B. J., Broccoli, A. J., & Hemler, R. S. (2004). On the use of cloud forcing to estimate cloud feedback. *Journal of Climate*, *17*(19), 3661–3665.

Stephens, G., Li, J., Wild, M., Clayson, C., Loeb, N., Kato, S., Andrews, T. (2012). An update on earth's energy balance in light of the latest global observations. *Nature Geoscience*, *5*(10), 691–696.

Stevens, B., Farrell, D., Hirsch, L., Jansen, F., Nuijens, L., Serikov, I., Prospero, J. M. (2016). The barbados cloud observatory: Anchoring investigations of clouds and circulation on the edge of the ITCZ. *Bulletin of the American Meteorological Society*, *97*(5), 787–801.

Taylor, K. E., Stouffer, R. J., & Meehl, G. A. (2012). An overview of CMIP5 and the experiment design. *Bulletin of the American Meteorological Society*, *93*(4), 485–498.

Tiedtke, M. (1989). A comprehensive mass flux scheme for cumulus parameterization in large-scale models. *Monthly Weather Review*, *117*(8), 1779–1800.

Tiedtke, M. (1993). Representation of clouds in large-scale models. *Monthly Weather Review*, *121*(11), 3040–3061.

Vanzanten, M., Stevens, B., Nuijens, L., Siebesma, A., Ackerman, A., Burnet, F., Wyszogrodzki, A. (2011). Controls on precipitation and cloudiness in simulations of trade-wind cumulus as observed during rico. *Journal of Advances in Modeling Earth Systems*, *3*, M06001. https://doi.org/10.1029/2011MS000056

Vial, J., Dufresne, J.-L., & Bony, S. (2013). On the interpretation of inter-model spread in CMIP5 climate sensitivity estimates. *Climate Dynamics*, *41*(11–12), 3339–3362.

Webb, M. J., Lock, A. P., Bodas-Salcedo, A., Bony, A., Cole, J. N. S., Koshiro, T., Stevens, B. (2015). The diurnal cycle of marine cloud feedback in climate models. *Climate Dynamics*, *44*(5–6), 1419–1436.

Zhang, M., & Bretherton, C. S. (2008). Mechanisms of low cloud-climate feedback in idealized single-column simulations with the community atmospheric model, version 3 (CAM3). *Journal of Climate*, *21*(18), 4859–4878.

Zhang, M., Bretherton, C. S., Blossey, P. N., Austin, P. H., Bacmeister, J. T., Bony, S., Zhao, M. (2013). CGILS: Results from the first phase of an international project to understand the physical mechanisms of low cloud feedbacks in single column models. *Journal of Advances in Modeling Earth Systems*, *5*, 826–842. https://doi.org/10.1002/2013MS000246